Available online at www.sciencedirect.com

Manufacturing Letters

Manufacturing Letters 00 (2023) 000–000

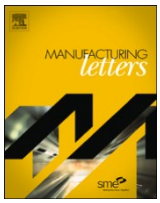

51st SME North American Manufacturing Research Conference (NAMRC 51, 2023)

A statistics of extremes-based method to predict the upper bound of geometrical defects in powder bed fusion

Panayiotis Kousoulas[a,b], Y.B. Guo[a,b,*]

[a]*Dept. of Mechanical and Aerospace Engineering, Rutgers University-New Brunswick, Piscataway, NJ 08854, USA*
[b]*New Jersey Advanced Manufacturing Institute, Rutgers University-New Brunswick, Piscataway, NJ 08854, USA*

* Corresponding author. Tel.: +1-848-445-2225; fax: +1-732-445-3124. *E-mail address:* yuebin.guo@rutgers.edu

Abstract

Geometrical defects (e.g., pores and lack of fusion) induced during powder bed fusion (PBF) pose a great challenge to fatigue performance for load-bearing structures. The random porosity may further cause uncertainty of fatigue behavior. Fatigue life and scattering bands are largely determined by the maximum size of a geometrical defect. Therefore, the prediction of the upper bound size of geometrical defects is critical. This work focuses on quantifying defect size and distribution to identify the extreme, life-limiting defect size that drives fatigue failure. A comprehensive analysis of the geometrical defects in PBF parts is presented. A statistics of extremes-based method is presented to predict the maximum defect. Defect size is measured using the Feret caliper (FC) diameter and then fitted to a cumulative distribution function (CDF) for linear regression modeling. The maximum defect size is then extrapolated from the regression line for a given probability. It is shown that multiple CDFs can be used for PBF defect size predictions, allowing for flexibility and optimization of prediction models. Furthermore, the FC diameter metric is proposed as the standard defect size metric due to its equivalent representation of 3D and 2D defects.

Keywords: Powder bed fusion; geometrical defects; statistics of extremes

1. Introduction

Metal additive manufacturing (AM) has great potential as a new industry standard for producing highly customizable metal components efficiently, with little to no tooling expense, and with less material waste than traditional manufacturing methods. Metal AM is revolutionary by allowing for on-demand manufacturing and decentralized production [1], making custom parts more accessible and readily available to consumers. It is thus of great interest to areas of industry that can benefit from easier and more cost-effective production of complex (often critical) components (e.g., aerospace, automotive, medical). There are limitations to this method, typically small production volumes and rates, and current metal AM processes have drawbacks like limited available materials, limited size of final parts, and lower surface quality [2].

Nomenclature

$\sqrt{area}$	Murakami defect size parameter
AM	additive manufacturing
CT	computed tomography
CDF	cumulative distribution function
FC	Feret caliper
LOF	lack of fusion
MLS	method of least squares
PBF	powder bed fusion
PDF	probability density function

1.1. Geometrical defects

The main metal AM processes, e.g., laser-based powder bed fusion (PBF) and directed energy deposition, use either a laser or an electron beam as the energy (heat) source to fuse metal particles or wires in a layer-by-layer progression on a metal substrate [3]. The process parameters and chamber environment and their variations affect the quality of the solidified part, as shown in many studies of process parameter effect on microstructure and properties of as-PBF parts (e.g., [4]). The geometrical flaws, including voids, cracks, warping, pores, or surface craters, and unwanted surface roughness in or on the as-printed part, are the most important quality factors. Technically, a defect renders a part defective. Some geometrical inhomogeneities are tolerable due to their relatively small size. Thus, as Snow et al. note [5] the term 'flaw' is more appropriate as a general label for pores and cracks. Since this paper focuses on critical flaws, the term 'defect' will be favored.

LPBF-induced geometrical defects can be grouped based on their methods of formation. As summarized by Snow et al. [5] these defects are 1) gas porosities, 2) melt pool instabilities (keyhole pores), and 3) regions with LOF. Gas pores are identified as nearly spherical voids within a printed part, and typically are the smallest in size of all three defect groups. These are introduced into the solidified metal either by the release of trapped gas inside the virgin (i.e., unmelted) powder stock or by gas bubbles enveloped by the melt pool. Melt pool instabilities result in voids and pores due to vaporization loss. At higher energy inputs, more molten metal from the melt pool can evaporate. This occurs when high energy source (e.g., laser) power and slow scanning speed parameters are used or when deceleration of the laser exposes the area of the powder bed incident to the energy source for more time. This results in a depression (keyhole) that collapses and creates voids at the keyhole bottom. LOF can occur systematically and stochastically, generally resulting in large, irregular voids, often identified by partially melted powder inside voids. Energy power and scanning parameters must be optimized to ensure subsequent scanning passes completely fuse new layers on top of previous layers. Even with optimized parameters, random LOF defects can still occur due to the highly volatile PBF process. Nearby unmelted powder can contaminate the melt pool as a spatter particles or by being blown by inert shielding gas, causing incomplete fusion.

Residual stresses develop in response to non-uniform heating and cooling [6] experienced by the solidified material during PBF. This can result in distortion of the part from the intended geometry and can weaken it through undesirable pre-loading that can prove fatal when additional loading is added [7]. Residual stresses also lead to defects, like cracks and delamination in the part, reducing its quality [8].

1.2. Geometrical defect characterization

The quality of PBF parts can be quantitatively characterized by measuring surface roughness, porosity, residual stress, and microstructure of the as-built part. Surface roughness can be mainly measured optically or with X-ray Computed Tomography (CT), and both approaches have been applied to studies of PBF parts. It is desirable to control these defects by optimizing process parameters, as has been studied extensively (e.g., [10]). Finding methods of predicting part quality is of great interest (e.g., [11, 12]).

The size and shape of a defect define its morphology (morph- from the Greek μορφή, or form). As discussed in the preceding section, the formation mechanism of a defect can be identified by its morphology. Thus, by characterizing defect geometry and location within a component, manufacturers can determine the root causes of any defect formation and tune their process parameters accordingly.

Morphology studies of internal defects originally required destructive methods (e.g., mechanical cutting) to investigate samples. By taking slices or sections of a sample, a 2D inspection area of the interior geometry can be observed by optical methods (e.g., [13]). While this method is relatively simple and easy for most investigators to perform, the nature of the destructive method of inspection does not leave the part intact for additional testing. This is not altogether unfavorable if simultaneous studies can be performed on the same sliced sample, e.g., microstructure formation and hardness. Yet, it still restricts morphology analysis to 2D descriptions of defect size and shape.

X-ray CT is a very popular non-destructive method of detecting internal cracks and porosity and measuring defect sizes [14]. While being very expensive and possibly time-consuming, CT can resolve the entire population of internal defects in each sample region and accurately portray not only 2D but also the 3D shape of defects with additional image processing. This allows direct 3D quantification of defects (e.g., population, volume fraction, sphericity, spatial orientation). Of course, the limiting size of defects that can be detected depends on the maximum resolution available, which can be on the order of tens of microns [15].

Juan et al. [16] presented a hybrid destructive and non-destructive investigative method for characterizing metal inclusions, first using scanning ultrasonic microscopy to detect the location of large internal defects and then dissecting the specimen to better observe the defects with scanning electron microscopy. While this does help to reduce the risk of missing or overlooking critical defects in a part, it lacks the advantage of 3D defect characterization.

3D representations of defects can be used to quantify the regularity or irregularity of defect shape. The measure of sphericity is the ratio of sphere surface area to defect surface area for a sphere with equal volume to the defect. Sphericity close to 1 represents near-spherical defects while low sphericity values denote irregular defects.

Equivalent diameter is a measure of 3D defect size, defined as the diameter of a sphere of equal volume [16]. This may not be suitable for elongated, irregular pores (e.g., LOF) since such defects may misrepresent how detrimental long, crack-like defects with relatively small areas can be to the fatigue performance of PBF components [17].

For 2D observations of defects, Murakami's $\sqrt{area}$ parameter [18] is a popular choice for representing defect size (e.g., [11, 19-22]), partly because it is used to predict the fatigue limit of PBF components. This parameter is defined as the

square root of the defect area normal to the direction of maximum tensile loading. This gives a 1D (length) measurement to represent the 2D (area) size of the defect. In some cases, defects are grouped closely together, making it difficult to assume the individual defects to be independent of or unaffected by the group [23]. This is because the material adjoining multiple defects may not offer any significant support under loading if there is very little of it. There are also times when defects are close enough to the part surface that the area between the defect and the surface does not offer much structural integrity. In these situations, an effective defect size [24] can be taken to estimate the total area affected by the sub-surface or interacting defects by drawing around the outer borders of the affected region to completely envelop all defects and/or the sub-surface defect area and the area immediately separating it from the free surface. Naturally, this requires the use of image analysis software, which is often included in optical measurement systems.

These methods are not intended to precisely measure actual defect size but rather estimate an effective crack length with approximately the same impact. This was explained by Murakami and Endo through their investigation comparing artificial defect holes with specific diameters to non-propagating cracks in steel specimens [25]. The level of precision of the measured area depends on how closely drawn the enveloping contour is to the actual boundaries of the defect. As mentioned by Oberreiter et al., higher precision can be more favorable for accurately depicting the actual defect area, which comes at the price of more complicated and tedious creation of the contours in image analysis software [21].

A possibly more accurate measurement of defect size is the maximum Feret caliper (FC) diameter [26]. The FC diameter measures the distance between two points across from each other on the boundary of interest and was used by Nicoletto et al. [14] in measuring the size of metallographically observed casting defects. The distribution of defect sizes was used in comparison to Murakami's $\sqrt{area}$ parameter to predict the maximum defect size, resulting in much larger predictions, yet well correlated, nonetheless. The predicted critical defect sizes using the FC diameter description also yielded closer approximations of the fatigue strength of cast AlSi7Mg. FC diameter also offers the flexibility of measuring defect size in 2D and 3D, which is analogous to measuring the diameter of a circumscribed circle or sphere.

1.3. Detrimental effect of geometrical defects

The effect of defects on the fatigue performance of PBF parts is a prominent area of research (e.g., [3, 24, 27, 28]). As seen with studies of high-strength steels, parts under dynamic loading can fail over time due to the growth of internal microcracks, which cause weakening to the point of fracture [13] through a fatigue process.

In bending fatigue, the applied stresses are highest at the surface of the specimen due to the stress gradient resulting from the elongation of one half of the specimen and compression on the opposing half. Any existing surface defects (e.g., surface roughness) will act as stress concentrations, which, for large enough stresses, will cause microcracks to propagate and eventually lead to specimen fracture. This is a major problem for as-built PBF materials, which inherently have high surface roughness from unmelted particles on the part surface and ridges from the staircase effect of the layer-by-layer building. This lowers the fatigue life and fatigue strength of the part from the ideal case of a smooth, unnotched specimen of the same geometry and material [29].

In the tension-compression mode, the applied stress is assumed to be uniform across the cross-section of the specimen, and fatigue fracture sites occur at the largest stress concentrations, irrespective of their depth from the surface [13]. This makes internal defects just as harmful as surface defects under this loading case.

It has been shown that post-processing surface finishing procedures (e.g., [30]) can be used to remove as-built surface roughness, which increases fatigue performance. Other post-processing methods, like hot isostatic pressing and heat treating, can increase the fatigue strength of PBF parts by eliminating or reducing the size of internal defects and relieving the part of residual stresses, respectively. However, post-processing methods do not solve the root cause of inferior fatigue performance. Post-processing is generally unfavorable because of the added time and expense to the manufacturing process. It is in the best interest of every manufacturer to minimize post-processing for increased efficiency and reduced cost. This involves refining AM processes to give optimal results with less porosity.

In discussing geometrical defects in AM specimens, Murakami et al. [29] explain that since individual specimens contain different defects in size, number, and location, the fatigue limit of a series of AM specimens is not constant (i.e., variable). The fatigue limit is the stress level below which microcracks do not propagate [18]. This means that the reliability of PBF components cannot be standardized with average values but rather with ranges of fatigue performance. The upper and lower bounds of fatigue strength of PBF materials provide a realistic measure of component performance that can be applied in engineering designs by quantifying the limitations of their use.

The uncertainty in the size, quantity, and distribution of these defects is not known. There is also a lack of understanding of the compound effect of defect factors on the fatigue performance of PBF parts. Manufacturers must therefore establish a threshold acceptance level for each quality factor of a printed part. For geometrical defects, this means establishing quality control methods for keeping maximum defect sizes at an acceptable level.

The objectives of this study are to 1) present a statistical methodology for predicting the maximum effective defect size in PBF material and 2) demonstrate the method through application to datasets of 2D and 3D defect sizes.

2. Statistics of extremes methodology

The prediction of extreme events has been studied in probability and statistics for many different applications. Extremes are rare events that are not often observed. It is a common problem in structural engineering to design buildings, bridges, and offshore structures to withstand extreme weather

events, such as large waves, strong wind gusts, flooding, and heavy snowfall.

The aim of the statistical theory of extreme values, in application to porosity, is to analyze observed pores in a printed sample and to forecast further extremes [31] (e.g., a maximum pore size). This can be done either through metallographic (destructive) examination or non-destructive methods (e.g., CT). The upper bound can be estimated probabilistically by extrapolating from the available data.

2.1. Random variables

The possibility of measuring or recording data of a specific value is called an event. Depending on the process of interest, event data is recorded as either a discrete random variable or a continuous random variable. For discrete data, there are a finite number of events. A realization occurs when an event happens.

Continuous random variables have infinite possibilities. The size of defects in PBF components is a continuous random variable. While there are limits to the possible defect sizes (defects cannot take up negative space or exceed the size of the actual component), there are a limitless number of possible sizes within these limits. Because of this, events of continuous random variables generally involve a range of possibilities since the possibility that one specific defect size is measured out of the infinite number of possibilities is close to zero.

2.2. Probability density and cumulative distribution functions

The probability density function (PDF) is a continuous description of how data from a given process is distributed over the corresponding range of possible values. This is analogous to a histogram plot of the data, which provides a discrete description. By fitting a PDF to available process data, the process behavior can be modeled analytically. To additionally model the probability, the cumulative distribution function (CDF) is needed. The CDF is the integral of the PDF. This is analogous to a cumulative frequency of a range of values. The range corresponds to the interval of integration over the PDF. As mentioned before, a range of values is considered for continuous random variables because the integration of a model PDF at one specific value will compute to zero.

The PDF and CDF are used together to quantify the behavior of continuous random variables by first matching data to a PDF and then applying the corresponding CDF to find the probability of realizing certain values. Fig. 1 gives an example plot of the well-known normal distribution, which has a PDF shaped like a bell. The continuous random variable is x. The shape of the curve is governed by the mean and standard deviation parameters of x. The CDF is superimposed in the same graph. For example, the probability of realizing x⩽4 is found as the area under the PDF curve from x=0 to x=4, or by solving the CDF for x=4. The probability of this event is relatively high since this encompasses a large area under the PDF.

In application to predicting extreme events, the values at the left and right tails of a PDF are of interest. These regions correspond to the extreme minima and maxima of distribution, respectively. While a CDF can output the probability for a given range of values, the inverse of the CDF can be used to solve for the values, given a probability. In this way, a prediction can be made about extreme values corresponding to a set probability.

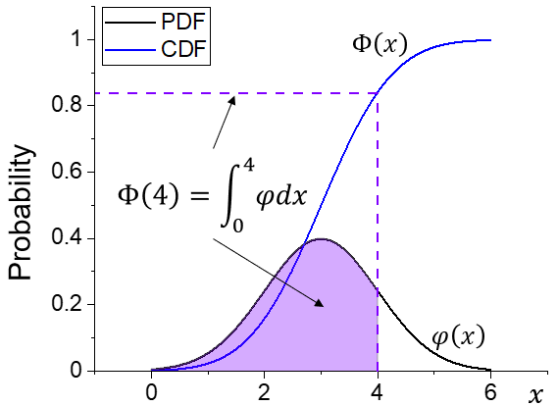

Fig. 1. Example plot of the normal distribution (PDF φ and CDF Φ) with mean 3 and standard deviation 1.

2.3. Statistical prediction methods for extreme values

The Type I Gumbel (maximum extreme values) distribution,

$$F(x) = \exp\left[-\exp\left(-\frac{x-\mu}{\sigma}\right)\right], \tag{1}$$

is often used to predict extreme defect sizes [15, 16, 32], where x is the defect size and μ and σ are shape parameters. This was popularized by Murakami [13] who initially applied statistics of extremes to nonmetallic inclusion defects observed by destructive sampling to predict $\sqrt{area}_{max}$, the maximum 2D inclusion size. The prediction method is graphically represented in Fig. 2 and is summarized as follows.

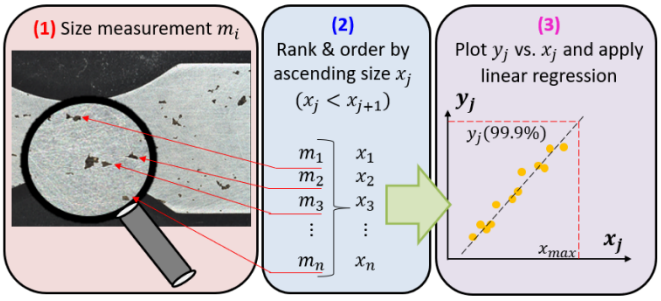

Fig. 2. Graphical procedure for predicting the maximum defect size.

First, the defect sizes x_j are ranked by $j = 1, 2, \ldots, n$ for n measured defects. Second, the reduced variate,

$$y_j = -\frac{x_j - \mu}{\sigma}, \tag{2}$$

is substituted in Eq. 1. Solving for y_j gives the expression for the inverse CDF as

$$y_j = -\ln[-\ln(F_j)], \quad (3)$$

where F_j is the cumulative probability of x_j being the true maximum defect based on the rank j,

$$F_j = \frac{j}{n+1}. \quad (4)$$

As the rank increases, the likelihood of the defect being the largest in existence increases. Third, y_j is plotted against x_j and linear regression (e.g., method of least squares, MLS) is applied. With the fitted line, a maximum defect size corresponding to a given probability (e.g., $F_{max} = 0.999$) can be extrapolated.

While Murakami's prediction method is well documented, it has become outdated as non-destructive characterization methods are becoming more popular than destructive methods. Furthermore, with the ability to characterize defect morphology in 3D there are multiple additional metrics to describe defect size. Researchers have also had success with other CDFs besides the Gumbel distribution in predicting defect size (e.g., [16, 22]). Therefore, a standard generalized methodology is proposed in the following section to accommodate different defect characterization and CDF model approaches. The proposed methodology is applied to predict the maximum defect size in PBF by giving step-by-step instructions.

3. Statistics of extremes for predicting the upper bound size of geometrical defects

3.1. Sample preparation

At least one material sample is needed for obtaining data on geometrical defects. Sufficient porosity must be measured to have an accurate representation of the total population of defects. Depending on the volume of the PBF samples and the sizes and quantity of defects, multiple samples may be required. Since the resulting porosity distribution depends on the process parameters used, defects from different material samples should not be considered in the same dataset unless those samples were made under identical conditions.

3.2. Defect characterization

The size of PBF defects should be quantified using the Feret caliper (FC) diameter metric to record the maximum dimension of defects (in either 2D or 3D inspection). Unless defects are connected, only individual defects should be measured, since multiple defects in close proximity do not necessarily represent the actual size of defects generated by the given PBF parameters. Multiple intersecting defects are measured as one single equivalent defect by measuring the diameter of the circle that circumscribes the intersecting defects. Additionally, sufficient data must be accumulated to capture the overall trend in the population distribution. It is recommended (at least for metallographic examinations) that defects on the order of hundreds be measured, based on a separate investigation on defect size distribution dependence on dataset size (see Fig. 3).

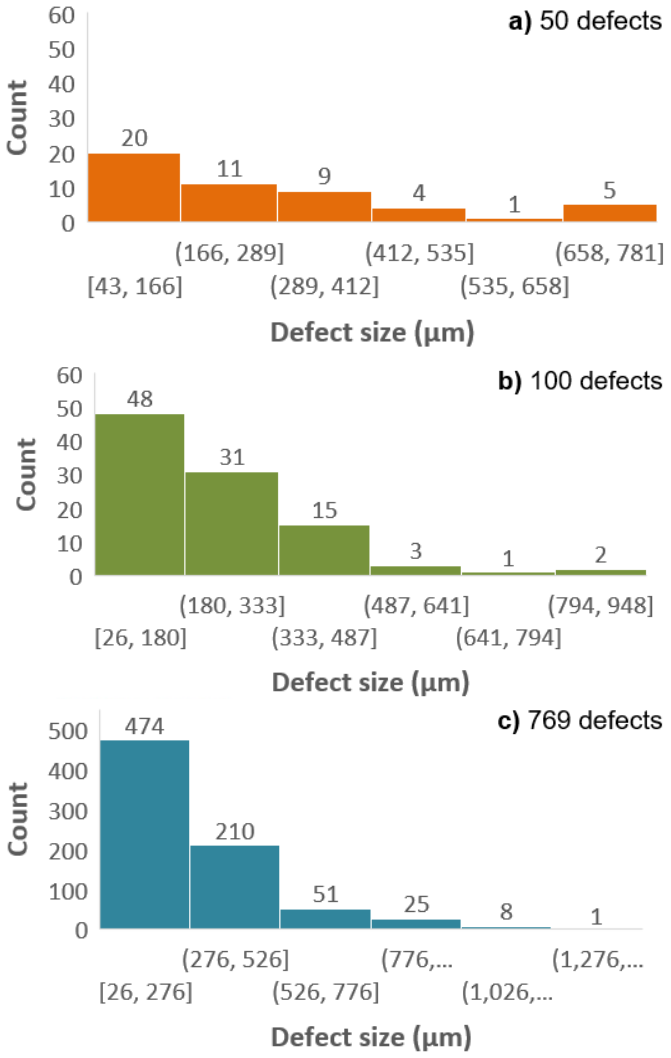

Fig. 3. Comparison of histograms of 50 randomly sampled and 100 randomly sampled PBF defect sizes from a total dataset of 769 defects measured metallographically by FC diameter. The largest defect measured 1526 µm.

3.3. Data preprocessing

The porosity data should be sorted in ascending size order, assigning each defect value a rank j, as described in section 2.3. A histogram of the data should be plotted to check the size distribution is right-skewed. The cumulative probability of each defect being the largest in existence is then calculated using Eq. 4.

3.4. Linear regression

A CDF (e.g., Gumbel, Exponential, Lognormal, Weibull, Generalized Extreme Values) must be chosen for linearly modeling the cumulative probabilities as a function of defect size. A reduced variate is used in place of the input variable and associated parameters (see Eq. 2). The inverse of the chosen CDF is used to solve for the reduced variate corresponding to each defect's cumulative probability. Then the reduced variates can be plotted against their corresponding defect sizes.

The resulting plot has a linear behavior. A regression line can then be applied using the method of least squares (MLS) and quantified by goodness-of-fit metrics (e.g., correlation coefficient). For the given probability of 99.9%, the maximum defect size can then be predicted by extrapolating from the regression line at the corresponding value of the reduced (see Fig. 2). This predicts that the resulting defect size has a probability of 99.9% of being the maximum.

It is important to note that depending on the CDF chosen, there may be parameters that have to be iterated to give the best regression. For example, the Weibull CDF,

$$\boldsymbol{F(x) = 1 - e^{-\left(\frac{x}{\alpha}\right)^{\gamma}}}, \quad \textbf{(5)}$$

has two parameters, α, and γ, with a reduced variate $y = \alpha/\gamma$ and an inverse CDF

$$\boldsymbol{y = [-\ln(1 - F)]^{1/\gamma}}. \quad \textbf{(6)}$$

An initial guess for γ gives an initial linear regression, which can then be tuned by iterating γ to obtain the best linear fit.

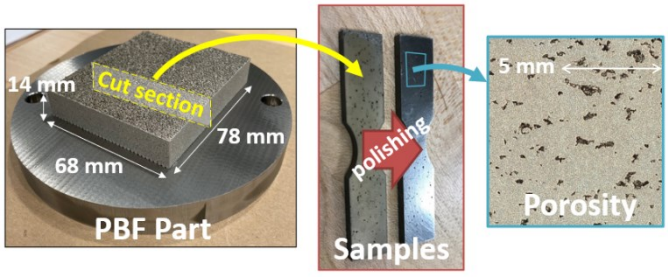

Fig. 4. Schematic of the sample preparation process.

4. Application to 2D and 3D defect data

The proposed methodology was applied to 2 separate experimental datasets of geometrical defects made by PBF. The first dataset is provided by the authors, containing 769 2D defects measured from a 316L stainless steel sample. The sample was printed to a height of 14 mm with the largest face (68 × 78 mm2) parallel to the substrate. Fig. 4 shows a schematic of the metrology preparation process. The SS-316L sample was sectioned using wire-electrical discharge machining to expose 28 inspection surfaces. Each inspection surface was then mechanically polished for observation by optical microscopy.

The second dataset was provided by researchers from the National Center for Additive Manufacturing Excellence (NCAME) of Auburn University who applied machine learning to classify 3D PBF defects obtained by CT [33]. The dataset consists of defect sizes measured using the major axis of a fitted ellipse (equivalent to the FC diameter). Details about the process parameters and porosity statistics for both datasets are given in Table 1.

The Gumbel and Weibull CDFs were both applied to predict the maximum defect size for each distribution of defects (see Eqs. 1 and 5). Fig. 5 compares the resulting predictions, which results in two important observations. First, both the Gumbel and Weibull CDFs can model the trend in the defect size distribution. This attests to the flexibility of the proposed method, showing that multiple functions can be used for probabilistic modeling. By testing different CDFs on the same data, an optimal model can be selected. In this case, comparing the predictions shows that the Gumbel CDF under-predicts the maximum defect size for both 2D and 3D defect distributions while the Weibull CDF gives realistic predictions in both cases. Thus, the flexibility of the proposed method enables optimization of the size prediction model.

Table 1. Process parameters and porosity statistics.

Defect Class	2D	3D
Material	SS-316L	Ti6Al4V
Porosity Statistics		
Dataset Size	769	464
Max (µm)	1525.9	96.6
Min (µm)	26.2	10.1
PBF Process Parameters		
Power (W)	250	336
Speed (mm/s)	800	780
Layer Height (µm)	50	40
Hatch Distance (µm)	70	120
Energy Density (J/mm^3)	89.3	89.7

The second important observation is the robustness of the FC diameter size metric, which can be used for both 2D and 3D defects. The popular $\sqrt{area}$ parameter metric is limited to 2D defect characterization. Furthermore, the more detailed characterizations of 3D defects have made it difficult to select a standard metric for quantifying defect size due to the many approaches explored in literature. The FC diameter metric is the ideal standard size metric simply due to its realistic and equivalent representation of defect size in both 2D and 3D cases.

5. Conclusions

Random porosity is a common geometrical defect in powder bed fusion (PBF) components. Understanding how to quantify the size and distribution of geometrical defects is key for assessing part quality and improving printing processes. In this study, a statistics of extremes-based method of predicting the maximum defect size is proposed. This method can be applied for both metallographic examinations as well as X-ray computed tomography inspections of porosity in PBF parts. Defect size is measured using the Feret caliper (FC) diameter and then fitted to a cumulative distribution function (CDF) for linear regression modeling. The maximum defect size is then extrapolated from the regression line for a given probability.

Future studies of defect size prediction should go further to consider the optimization of CDF selection for different process parameters and defect populations. Furthermore, the FC diameter metric should be accepted as the standard defect size metric in AM metrology methods due to its equivalent representation of 3D and 2D defects.

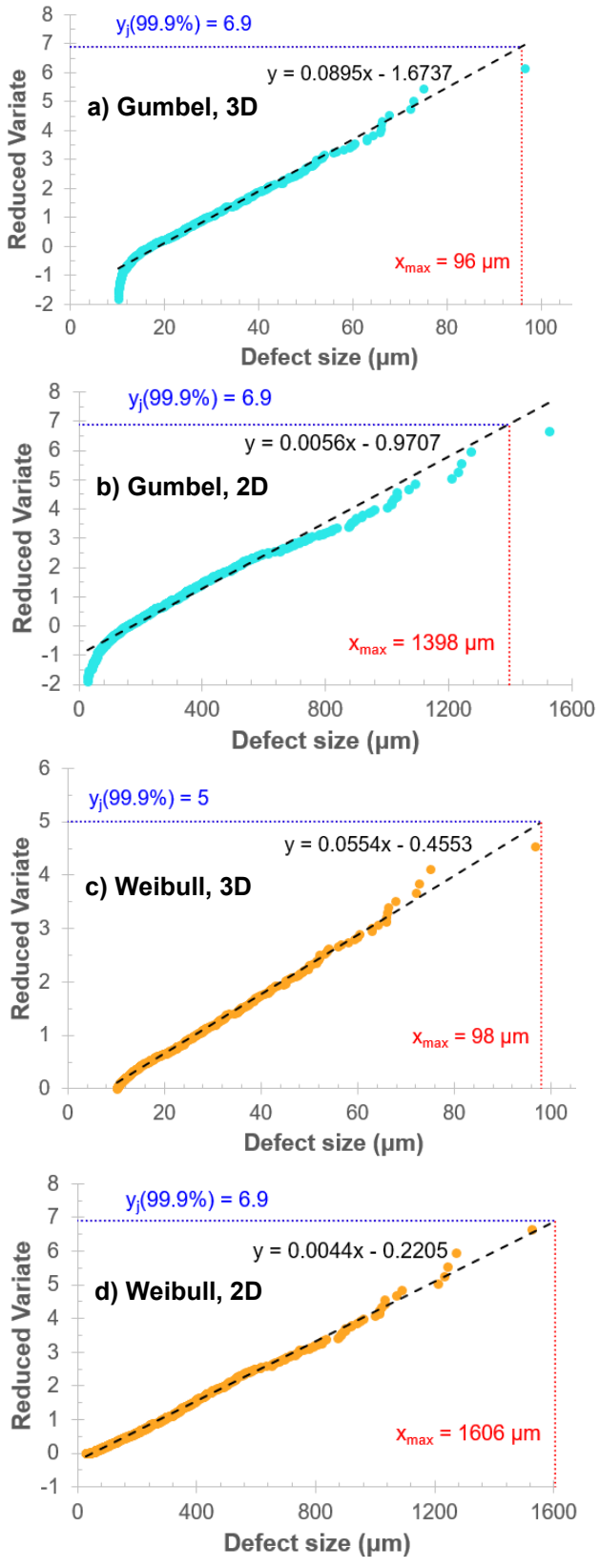

Fig. 4. Predicted maximum defect sizes at 99.9% probability using Gumbel and Weibull CDFs. a) Gumbel prediction for 3D defect distribution, b) Gumbel prediction for 2D defect distribution, c) Weibull prediction (parameter γ=1.2) for 3D defect distribution, d) Weibull prediction (parameter γ=1) for 2D defect distribution.

Acknowledgments

The authors would like to thank the financial support of the National Science Foundation under the grant CMMI- 2152908. Additional thanks to the NCAME researchers for graciously sharing their data on 3D defect sizes.

References

[1] Attaran M. The rise of 3-D printing: The advantages of additive manufacturing over traditional manufacturing. in Business horizons vol. 60, ed; 2017. pp. 677-688.
[2] Rosen DKim S. Design and Manufacturing Implications of Additive Manufacturing. in Journal of materials engineering and performance vol. 30, ed; 2021. pp. 6426-6438.
[3] Sanaei NFatemi A. Defects in additive manufactured metals and their effect on fatigue performance: A state-of-the-art review. in Progress in Materials Science vol. 117, ed; 2021. p. 100724.
[4] Kamath C, El-Dasher B, Gallegos GF, King WESisto A. Density of additively-manufactured, 316L SS parts using laser powder-bed fusion at powers up to 400 W. in The International Journal of Advanced Manufacturing Technology vol. 74, ed; 2014. pp. 65-78.
[5] Snow Z, Nassar ARReutzel EW. Invited Review Article: Review of the formation and impact of flaws in powder bed fusion additive manufacturing. in Additive Manufacturing vol. 36, ed; 2020. p. 101457.
[6] Callister Jr. WDRethwisch DG, Materials Science and Engineering: An Introduction, 8 ed. Hoboken, NJ, USA: John Wiley and Sons, Inc. , 2010.
[7] Edwards PRamulu M. Fatigue performance evaluation of selective laser melted Ti–6Al–4V. in Materials Science and Engineering: A vol. 598, ed; 2014. pp. 327-337.
[8] Pant P, Proper S, Luzin V, Sjöström S, Simonsson K, Moverare J, Hosseini S, Pacheco VPeng RL. Mapping of residual stresses in as-built Inconel 718 fabricated by laser powder bed fusion: A neutron diffraction study of build orientation influence on residual stresses. in Additive Manufacturing vol. 36, ed; 2020. p. 101501.
[9] Mohr G, Altenburg SJ, Ulbricht A, Heinrich P, Baum D, Maierhofer CHilgenberg K. In-Situ Defect Detection in Laser Powder Bed Fusion by Using Thermography and Optical Tomography—Comparison to Computed Tomography. in Metals vol. 10, ed; 2020. p. 103.
[10] Koutiri I, Pessard E, Peyre P, Amlou ODe Terris T. Influence of SLM process parameters on the surface finish, porosity rate and fatigue behavior of as-built Inconel 625 parts. in Journal of Materials Processing Technology vol. 255, ed; 2018. pp. 536-546.
[11] Deng H, Liu Q, Liu HYu H. Long-Life Fatigue of Carburized 12Cr2Ni Alloy Steel: Evaluation of Failure Characteristic and Prediction of Fatigue Strength. in Metals vol. 8, ed; 2018.
[12] Mukherjee TDebRoy T. Mitigation of lack of fusion defects in powder bed fusion additive manufacturing. in Journal of Manufacturing Processes vol. 36, ed; 2018. pp. 442-449.
[13] Murakami Y. Inclusion Rating by Statistics of Extreme Vlaues and Its Application to Fatigue Strength Prediction and Quality Control of Materials. in Journal of Research of the National Institute of Standards and Technology vol. 99, ed; 1994. pp. 345-351.
[14] Nicoletto G, Konečná RFintova S. Characterization of microshrinkage casting defects of Al–Si alloys by X-ray computed tomography and metallography. in International journal of fatigue vol. 41, ed; 2012. pp. 39-46.
[15] Romano S, Brandão A, Gumpinger J, Gschweitl MBeretta S. Qualification of AM parts: Extreme value statistics applied to tomographic measurements. in Materials & design vol. 131, ed; 2017. pp. 32-48.
[16] Juan R, Wang M, Lian J, Gu C, Li LBao Y. Quantifying the Comprehensive Characteristics of Inclusion-Induced Defects Using an Integrated Destructive and Non-Destructive Method. in Materials vol. 14, ed; 2021. p. 1475.
[17] Hastie JC, Kartal ME, Carter LN, Attallah MMMulvihill DM. Classifying shape of internal pores within AlSi10Mg alloy manufactured by laser powder bed fusion using 3D X-ray micro computed tomography: Influence of processing parameters and heat treatment. in Materials Characterization vol. 163, ed; 2020. p. 110225.

[18] Yukitaka MMasahiro E. Quantitative evaluation of fatigue strength of metals containing various small defects or cracks. in Engineering Fracture Mechanics vol. 17, ed; 1983. pp. 1-15.
[19] Wu Z, Wu S, Bao J, Qian W, Karabal S, Sun WWithers PJ. The effect of defect population on the anisotropic fatigue resistance of AlSi10Mg alloy fabricated by laser powder bed fusion. in International journal of fatigue vol. 151, ed; 2021. p. 106317.
[20] Nadot Y, Nadot-Martin C, Kan WH, Boufadene S, Foley M, Cairney J, Proust GRidosz L. Predicting the fatigue life of an AlSi10Mg alloy manufactured via laser powder bed fusion by using data from computed tomography. in Additive Manufacturing vol. 32, ed; 2020. p. 100899.
[21] Oberreiter M, Fladischer S, Stoschka MLeitner M. A Probabilistic Fatigue Strength Assessment in AlSi-Cast Material by a Layer-Based Approach. in Metals vol. 12, ed; 2022. p. 784.
[22] Anderson CW, Shi G, Atkinson HV, Sellars CMYates JR. Interrelationship between statistical methods for estimating the size of the maximum inclusion in clean steels. in Acta materialia vol. 51, ed; 2003. pp. 2331-2343.
[23] Yamashita Y, Murakami T, Mihara R, Okada MMurakami Y. Defect analysis and fatigue design basis for Ni-based superalloy 718 manufactured by selective laser melting. in International journal of fatigue vol. 117, ed; 2018. pp. 485-495.
[24] Masuo H, Tanaka Y, Morokoshi S, Yagura H, Uchida T, Yamamoto YMurakami Y. Influence of defects, surface roughness and HIP on the fatigue strength of Ti-6Al-4V manufactured by additive manufacturing. in International Journal of Fatigue vol. 117, ed; 2018. pp. 163-179.
[25] Murakami YEndo T. Effects of small defects on fatigue strength of metals. in International Journal of Fatigue vol. 2, ed; 1980. pp. 23-30.
[26] Wang QGJones PE. Prediction of Fatigue Performance in Aluminum Shape Castings Containing Defects. in Metallurgical and Materials Transactions B vol. 38, ed; 2007. pp. 615-621.
[27] Shrestha R, Simsiriwong JShamsaei N. Fatigue behavior of additive manufactured 316L stainless steel under axial versus rotating-bending loading: Synergistic effects of stress gradient, surface roughness, and volumetric defects. in International Journal of Fatigue vol. 144, ed; 2021.
[28] Murakami Y, Masuo H, Tanaka YNakatani M. Defect Analysis for Additively Manufactured Materials in Fatigue from the Viewpoint of Quality Control and Statistics of Extremes. in Fatigue Design, ed; 2019. pp. 113-122.
[29] Murakami Y, Takagi T, Wada KMatsunaga H. Essential structure of S-N curve: Prediction of fatigue life and fatigue limit of defective materials and nature of scatter. in International Journal of Fatigue vol. 146, ed; 2021.
[30] Alfieri V, Argenio P, Caiazzo FSergi V. Reduction of Surface Roughness by Means of Laser Processing over Additive Manufacturing Metal Parts. in Materials (Basel) vol. 10, 2017/08/05 ed; 2016.
[31] Gumbel EJ, "Statistics of Extremes." New York, NY, USA: Columbia University Press, 1957, pp. 1-36, 82, 113, 156-159.
[32] Hu YN, Wu SC, Wu ZK, Zhong XL, Ahmed S, Karabal S, Xiao XH, Zhang HOWithers PJ. A new approach to correlate the defect population with the fatigue life of selective laser melted Ti-6Al-4V alloy. in International journal of fatigue vol. 136, ed; 2020. p. 105584.
[33] Poudel A, Yasin MS, Ye J, Liu J, Vinel A, Shao S, Shamsaei N. Feature-based volumetric defect classification in metal additive manufacturing. in Nature Communications vol. 13, ed; 2022.